



CHORUS

This is the accepted manuscript made available via CHORUS. The article has been published as:

Persistence of force networks in compressed granular media

M. Kramar, A. Goulet, L. Kondic, and K. Mischaikow
Phys. Rev. E **87**, 042207 — Published 22 April 2013

DOI: [10.1103/PhysRevE.87.042207](https://doi.org/10.1103/PhysRevE.87.042207)

Persistence of Force Networks in Compressed Granular Media

M. Kramar¹, A. Goulet², L. Kondic², K. Mischaikow¹

¹*Department of Mathematics, Rutgers University, Piscataway, NJ 08854-8019*

²*Department of Mathematical Sciences, New Jersey Institute of Technology, Newark, NJ 07102*

(Dated: April 7, 2013)

We utilize the tools of persistent homology to analyze features of force networks in dense granular matter, modeled as a collection of circular, inelastic frictional particles. The proposed approach describes these networks in a precise and tractable manner, allowing to identify novel features which are difficult or impossible to characterize by other means. In contrast to other techniques that consider each force threshold level separately, persistent homology allows us to consider all threshold levels at once to describe the force network in a complete and insightful manner. We consider continuously compressed system of particles characterized by varied polydispersity and friction in two spatial dimensions. We find significant differences between the force networks in these systems, suggesting that their mechanical response may differ considerably as well.

PACS numbers: 45.70.Qj, 45.7-.Vn, 45.70.-n, 83.80.Fg

I. INTRODUCTION

Force networks play a key role in determining mechanical properties of static and dynamic dense granular media (DGM). The networks of particles connected by strong (larger than average) forces form a backbone of so-called ‘force chains’ that are considered to be responsible for load bearing [1]. These networks are frequently studied. The analysis of associated force distributions is the most common treatment, see e.g. [2]. Force network ensemble approach has been put forward recently; see [3] for a review. Also, first attempts have been made towards quantifying the structure of force networks. In [4] an effort was made to define the force chains from a local, particle-scaled point of view. More globally, the force networks were claimed to be universal and characterized by a set of critical parameters [5]. A complex network type of analysis, exploring stability of the force networks has been considered as well recently, see [6–8] and the references therein.

Despite significant progress, the analysis of the force network is still limited by the complexity of the problem, and the need to answer a particular set of questions of relevance to DGM. We note that in numerical simulations [9] and in principle in controlled experiments [2], complete information about the forces at the contacts between the particles is available. However, this information is too voluminous to be of direct use. The network-type of analysis provides useful information about stability [8], but it does not provide detailed information about force network structure. Probability density function tells us what is the probability of having large forces in a system, see, e.g., [1, 2, 10–12], but not about connectivity of the force network. While the suggestion about universal properties of the force networks is intriguing, it is known that their properties (distribution of forces for example) is strongly influenced by the particle friction and polydispersity [13]. This information is not encoded in the critical parameters. Therefore, it is necessary to consider alternative approaches to describe the force net-

works in the manner which is concise, but insightful, and accounts for both similarities and differences between the systems considered. Furthermore, it is of interest to develop an approach which is applicable to both static and dynamic settings, which in principle could be applied to particles of irregular shapes, and which is not limited by physical dimensionality of the system.

In this paper we present a novel approach that provides a simple set of measures describing properties of force networks in a selected set of granular systems. This proposed set of measures allows to distinguish between different systems and can be used to identify and predict their properties. In addition, we show that the information obtained using this set of measures may be difficult or impossible to obtain using some of the standard measures for analyzing granular systems.

To introduce the proposed approach consider the magnitude of the force field as a continuous scalar field $f: X \rightarrow [0, \infty)$. [In this work we concentrate only on the normal forces between particles; additional information that may be obtained based on tangential forces will be discussed elsewhere.] The space X is the union of the granular particles. A threshold $\theta \in [0, \infty)$ is chosen and the force network FN is defined to be the set of points on which the magnitude of the force exceeds the threshold, $\text{FN}(f, \theta) = \{x_i \mid f(x_i) \geq \theta\}$. The general goal is to describe the geometry of $\text{FN}(f, \theta)$.

The choice of a particular threshold level θ is somewhat arbitrary and thus it is desirable to describe the geometry of $\text{FN}(f, \theta)$ for all thresholds. Persistent homology [14, 15], described below, is a relatively new mathematical tool that allows to consistently relate the geometry of force networks over ranges of thresholds. This provides deeper insight than looking only at the number of clusters/components described by Betti numbers [13], or, more commonly by the tools of percolation theory.

The rest of this paper is described as follows. Section II describes the methods used, with a significant amount of information given in Appendices A and B regarding discrete element simulation and persistence techniques,

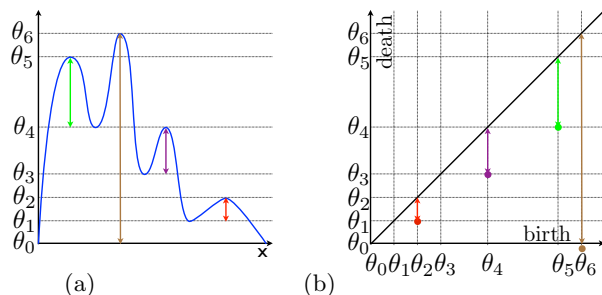


FIG. 1: (Color online)(a) An example of scalar field. Geometric features are indicated by the arrows. (b) The associated persistence diagram. Points correspond to the features indicated by the arrows of the same length and color.

respectively. The main results obtained using persistence analysis are given in Sec. III A, while the results obtained using more classical approaches are in Sec. III B. We conclude in Sec. IV.

II. METHODS

A. Discrete Element Simulations (DES)

The simulations are of the type utilized in [13]; for completeness, a brief outline is given in Appendix A.

We consider a square domain in 2D where $N \approx 2000$ granular particles are constrained between four rough walls made out of monodisperse particles. The walls move with constant prescribed speed, allowing to consider packing fractions, ρ , in the range [0.6 : 0.9]. The particles are inelastic frictional polydisperse discs, with the radii varying randomly in some range $1 \pm r_p/2$ in units of average particle diameter. All the results are obtained as averages over 20 realizations characterized by different initial conditions. In addition to the averages, we calculated standard deviations, and found them to be at least an order of magnitude smaller, suggesting that 20 realizations are sufficient to obtain statistically significant results.

B. Algebraic Topology

Homology provides an easily computable, rigorous, systematic, dimension independent means of characterizing geometric structures of spaces via a few integers β_* called *Betti numbers*; in 2D only β_0 , the number of distinct components, and β_1 , the number of closed loops, are relevant; β_0 and β_1 are related to the metrics used in [5] and [7].

Our first goal is to understand the structure of $\text{FN}(f, \theta)$ as a function of the force field f and the threshold θ . Persistent homology quantifies how this structure changes as one moves from high to low thresholds.

Figure 1 illustrates the approach using an one dimensional (1D) example. The set $\text{FN}(f, \theta) = \emptyset$ for $\theta > \theta_6$ and

	$\mu = 0.0$				$r_p = 0.4$			
r_p	0.0	0.1	0.2	0.4	μ	0.0	0.2	0.5
ρ_c	0.8615	0.8448	0.8282	0.8140	ρ_c	0.8140	0.7962	0.7884

TABLE I: ρ_c determined by the average number of contacts $Z(\rho_c) = 3$. Similar values are found if inflection points of the $Z(\rho)$ curves are used [13].

it consists of one connected component for $\theta \in (\theta_5, \theta_6]$. Another connected component appears at the level θ_5 . This component merges with the first one at θ_4 . In language of persistent homology a geometric feature indicated by the green arrow between θ_4 and θ_5 in Fig. 1(a) was born at θ_5 and died at θ_4 . This event is captured by the green point (θ_5, θ_4) in Fig. 1(b). Analogously the other two features indicated by the purple (θ_3, θ_4) and red (θ_1, θ_2) arrow are captured by the corresponding points in Fig. 1(b). The first connected component which appeared at θ_6 persists for all $\theta < \theta_6$ and is represented by the brown point with the birth coordinate θ_6 and a negative death coordinate. The negative value indicates that the feature persisted for all $\theta < \theta_6$.

Note that in our 1D example $\beta_0(f, \theta) = 2$ for $\theta \in (\theta_3, \theta_5]$. However, significant geometric change occurred at θ_4 . Two components merged – equivalently one component *died* – and a new component appeared – was *born*. Persistent homology makes precise the notion of birth and death of geometric features; in particular it associates a birth threshold θ_b for which the feature appears in the set $\text{FN}(f, \theta_b)$, and a death threshold θ_d , $\theta_b > \theta_d$, for which the feature disappears in the set $\text{FN}(f, \theta_d)$. The collections of these points $(\theta_b, \theta_d) \in \mathbb{R}^2$, one for β_0 and the other for β_1 (in 2D), form the *persistence diagrams*. More detailed description is given in Appendix B.

C. Binning of Forces

We will see in the following section that the persistence diagrams computed from the DES results are significantly more complex than the 1D example considered above, and some approach to quantifying the information contained in the diagrams is needed. The approach that we will consider here is based on ‘binning’ the forces in the separate parts of the persistence diagrams. This approach is described next.

Let \bar{F} denote the average contact force, and consider the region $[0, 5\bar{F}]$. If the force is larger than $5\bar{F}$ we redefine it to be $5\bar{F}$ (this occurs rarely). We ignore the loops which arise from three particles coming into contact. Alternative approaches that consider loops made out of three or more particles have been considered recently [7, 16]. For the purpose of discussion that follows, we define a *defect* to be a minimal loop defined by four or more particles (the number of defects describes departure from a perfect crystal).

Using the DES results, at each time (corresponding to a given packing fraction, ρ), we compute two persistence diagrams using Perseus [18, 19]. In order to help the

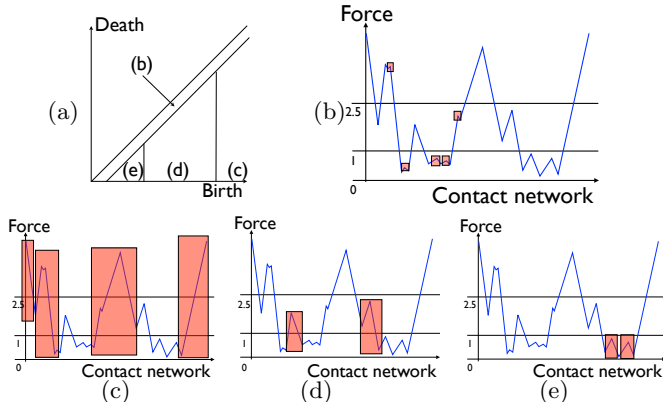


FIG. 2: (Color online) (a) Bins in persistence diagram. (b)-(e) Examples of geometric features corresponding to the points in the (b) rough, (c) strong, (d) medium and (e) weak b_0 bins.

interpretation, we bin the points (θ_b, θ_d) into four disjoint regions: *Rough*: $(\theta_b - \theta_d) < 0.1\bar{F}$; *Strong*: $\theta_b \geq 2.5\bar{F}$; *Medium*: $\bar{F} \leq \theta_b < 2.5\bar{F}$; *Weak*: $0.1\bar{F} \leq \theta_b < \bar{F}$, which can be briefly interpreted as follows (see also Fig. 2).

- β_0 Rough: This is generated by a contact of a force θ_b that is a local maximum of the force field. The associated component contains the contact of a force θ_d which is a saddle or a local minimum of the force field. Since $\theta_b - \theta_d < 0.1$ is small, this suggests that this geometric feature represents local, fine structure of the force field (roughness).

- β_0 Strong (and similarly for medium, weak): $\theta_b \geq 2.5\bar{F}$ and $(\theta_b - \theta_d) \geq 0.1\bar{F}$. This is generated by a contact of a strong force and the associated component extends through a reasonable range of values.

- β_1 Rough: $(\theta_b - \theta_d) < 0.1\bar{F}$. This is generated by a loop of adjacent particles for which the contact experiences the force θ_b . If $\theta_b > 0.1\bar{F}$, then within the loop there are no defects and the contact with the lowest force within the loop experiences the force θ_d .

- β_1 Strong (and similarly for medium, weak): $\theta_b \geq 2.5\bar{F}$ and $(\theta_b - \theta_d) \geq 0.1\bar{F}$. A loop for which the weakest contact experiences an exceptionally strong force. If $\theta_d > 0$, then there are no defects within the loop.

III. RESULTS

A. Persistence Analysis of the Force Field in DGM

Figure 3 shows two examples of force networks (normal forces only) that we consider. The snapshots are taken just before jamming. Figure 3(a) documents the emergence of organized structure for the frictionless monodisperse system at $\rho \sim 0.86$. The hexagonal structure clearly visible in the lower left part of the domain extends to a large part of the domain and forms an imperfect crystal as ρ increases. On the other hand the polydisperse system ($r_p = 0.4$) with the friction coefficient $\mu = 0.5$ displays no ordering; see also [13] for further discussion

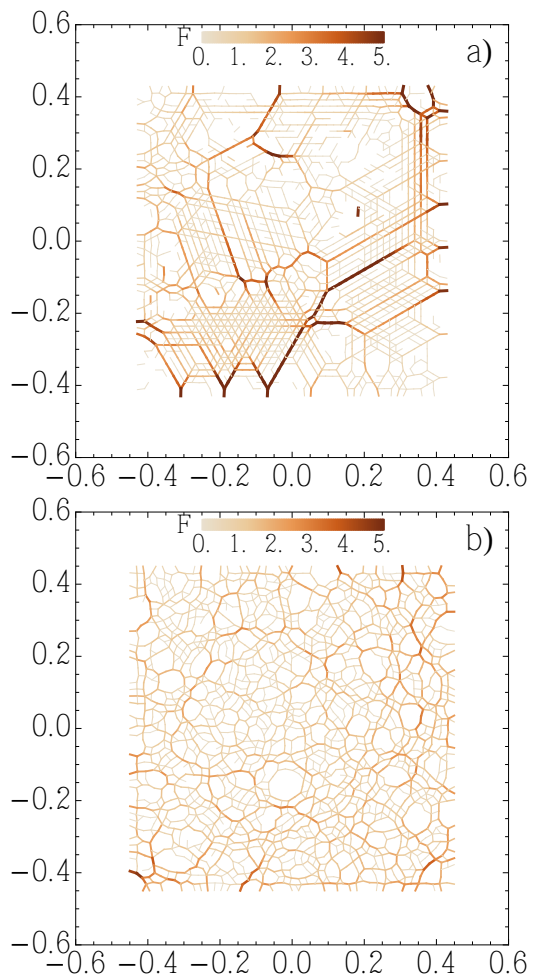


FIG. 3: (Color online) Force field near jamming for a) monodisperse frictionless system at packing fraction $\rho \sim 0.86$ and b) polydispersity $r_p = 0.4$ with friction coefficient $\mu = 0.5$ at packing fraction $\rho \sim 0.78$. Animations that include corresponding persistence diagrams are available [17].

of this point. Figure 4 shows the persistence diagrams for the two examples shown in Fig. 3. The evolution of the force networks and of persistence diagrams as systems are being compressed can be also seen in the linked animations [17].

For the persistence analysis, we consider 20 realizations for each considered system, and extract normal contact forces at ≈ 100 values of ρ and compute eight functions $N_i^*(\rho)$ which indicate the number of β_i persistence points in bin $*$, where $*$ $\in \{R, S, M, W\}$ (denoting Rough, Strong, Medium and Weak). The results that follow are robust with respect to the exact definitions of the binning regions. The effects of the compression speed turn out to be minor and will be discussed elsewhere, as well as the influence of system size.

Figure 5 shows $N_i^*(\rho)$ for frictionless particles and ρ in the interval $[0.73, 0.9]$. [For $\rho \in [0.6, 0.73]$ the systems are indistinguishable and characterized by large values of N_0^R (Figure 5(a)) and relatively small values of $N_0^{S,M,W}$.

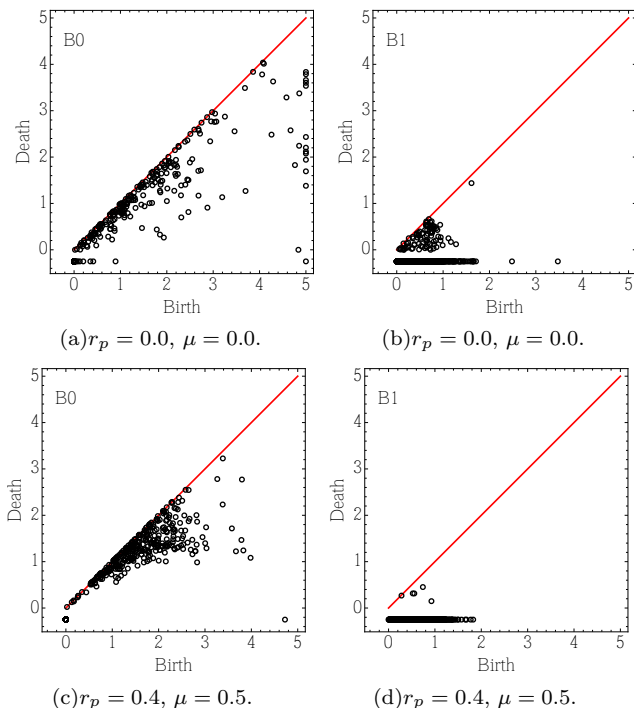


FIG. 4: (Color online) Persistence diagrams for the examples shown in Fig. 3.

Since $N_0^R \approx N$, this suggests that particles are typically separated with occasional interactions, as expected.] The leftward shift of N_i^* as r_p is increased is due to the fact that ρ_c , the packing fraction at which jamming occurs (see Table I), is a decreasing function of r_p . Observe that as a function of ρ , N_0^W (Figure 5(d)) gradually increases and then sharply decreases. This can be explained as follows: as the system is compressed there is less freedom for movement of particles and thus contacts develop into weak components. However, there is still enough freedom for rearrangement of the contacts, thus over this range the number of weak components dominates the number of strong or medium ones. As the system approaches jamming and the freedom disappears, the structure of the force networks changes dramatically. First there is a rapid rise in $N_0^{S,M,W}$ followed by the collapse of N_0^W and the continued rise of $N_0^{S,M}$ for a range of ρ 's beyond ρ_c . The latter occurs due to transfer of components from weak to medium and strong, suggesting that the force network continues to steepen even after jamming.

Figure 5 shows also N_1^* curves, which give information about the loops that form in force networks. These curves show that the loop formation is closely related to jamming, with a rapid increase in $N_1^{M,W}$ beginning just before and continuing shortly after ρ_c .

There is additional, less expected information provided by persistent homology. That $N_0^R(\rho)$ decreases to rather low values for $\rho > \rho_c$ indicates that in a jammed state the force field is 'smooth,' that is there are relatively few small variations in the magnitude of force even in

the presence of significant fluctuations as measured by N_0^M . Similarly, there are very few strong loops, N_1^S , and these loops are essentially expected only in monodisperse systems. Recall that slowly compressed frictionless systems of monodisperse particles crystallize (see [13] for discussion regarding influence of crystallization on Betti numbers). We conjecture that the maximum of $N_1^{S,W}$ for $r_p = 0$ characterizes the value of ρ at which crystallization occurs. This is supported by measurement of the bond orientation factor, ψ_6 , discussed later in the text, and by visual inspection of force networks, see Fig. 3. The latter shows that these strong loops form at the fault lines between crystalline zones. Furthermore, the sharp global maxima in $N_1^{S,W}$ and a change in slope to a steeper rise in N_1^M after crystallization suggests a 'balancing' of the load of the system and hence the decrease in the variance in the magnitude of the force. The observation that N_0^S attains a maximum after ρ_c while N_0^M is ever increasing is consistent with this concept of balancing. It also provides an explanation for the fact that N_0^S is larger for $r_p = 0.1$ than $r_p = 0$; the lack of broad perfect crystalline regions allows for larger variation in the force field. This 'perturbative' explanation does not extend to larger r_p since the crystalline structure no longer exists. This suggests that *there is a critical $r_p^{crit} \neq 0$ at which the number of strong maxima in the force network is the largest.*

Next, we proceed to discuss the influence of friction. Figure 6 compares three polydisperse systems, $r_p = 0.4$, characterized by different Coulomb threshold, μ , and demonstrates that persistent homology provides a mean of measuring the strong influence of friction on the geometry of force networks. The most pronounced and crucial feature is that $N_0^{S,W}(\rho_c)|_{\mu=0} \gg N_0^{S,W}(\rho_c)|_{\mu>0}$. This finding says that *the force network features in frictionless systems around jamming point are extreme, compared to frictional systems.* This observation should be contrasted with the ones of [13] which were based purely on Betti number computations (thus measuring the contact network) and did not capture this difference. *The conclusion is that force networks' properties are not simply slaved to the contact network.*

B. Classical Approaches to Analysis of the Force Field in DGM

We now turn to the question of how the findings formulated so far relate to the ones obtained by other well established measures. Let us first consider the measures based on particles' spatial distribution. Figure 7 shows the pair correlation, $g(d)$, as a function of distance in units of average particle diameter for a large packing fraction, $\rho = 0.9$. The results are again obtained by averaging over 20 simulations for each given set of physical parameters. The pair correlation function for frictionless systems with several polydispersities, r_p , is depicted in Fig. 7(a). The results for monodisperse frictionless system suggest a well defined crystal structure

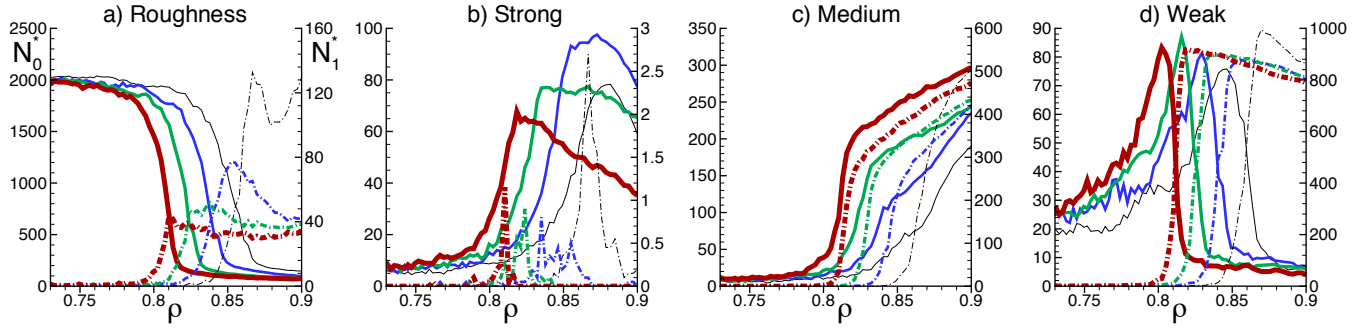


FIG. 5: (Color online) Number of generators, N_0 (left y -axes, solid lines) and N_1 (right y -axes, dashed lines) as a function of ρ for the systems characterized by zero friction ($\mu = 0$) and polydispersities $r_p = 0$ (thin, black), $r_p = 0.1$ (thicker, blue), $r_p = 0.2$ (even thicker, green), and $r_p = 0.4$ (thickest, magenta).

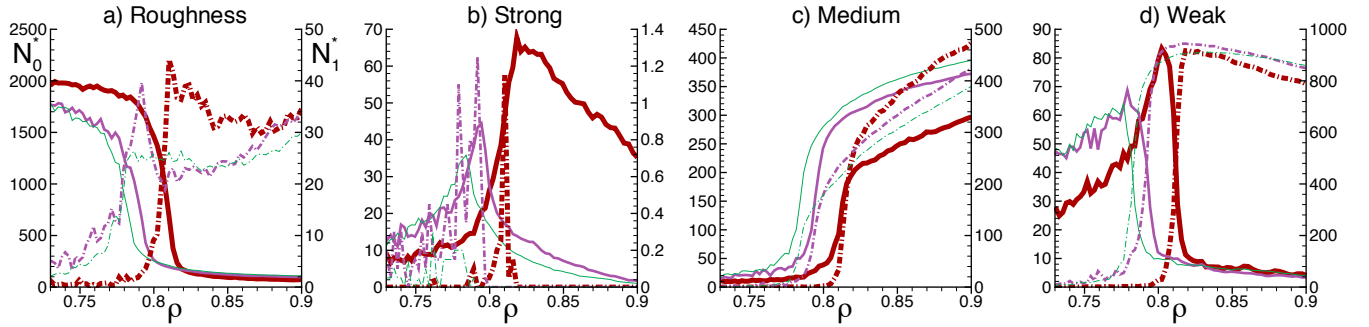


FIG. 6: (Color online) Number of generators, N_0^* (left y -axes) and N_1^* (right y -axes) as a function of ρ (horizontal axis) for the polydisperse ($r_p = 0.4$) systems characterized by different Coulomb friction coefficient: $\mu = 0$ (thickest, magenta) $\mu = 0.2$ (thinner, purple), $\mu = 0.5$ (thinnest, green). Note different ranges in the y -axes compared to Figure 5.

for $\rho = 0.9$. Fig. 7(a) implies that the system becomes disordered with no distinctive features for $r_p > 0.1$. Furthermore, Fig. 7(b) suggests lack of long-range order for polydisperse systems with $r_p = 0.4$ regardless of the friction coefficient, μ .

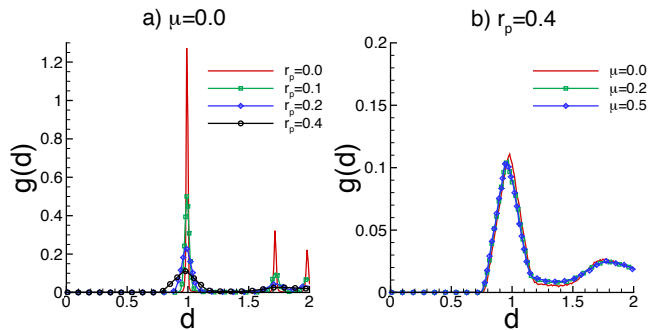


FIG. 7: (Color online) Pair correlation function at $\rho = 0.9$ for a) frictionless system as polydispersity, r_p , is varied, and b) polydisperse, $r_p = 0.4$ system, as friction coefficient, μ , is varied. Here the distance is measured in average particle diameters, and g is in arbitrary units.

Additional information can be obtained by considering bond orientational order parameter, ψ_6 , defined by

$$\psi_6 = \left\langle N^{-1} \sum_{j=1}^N (N_b - 1)^{-1} \sum_{k=1}^{N_b-1} \cos(6\theta_k) \right\rangle$$
, where N_b is the number of contacts/bonds for a particle j , and θ_k is the angle between two consecutive bonds. We denote by $\langle \cdot \rangle$ the average over 20 simulations. For a

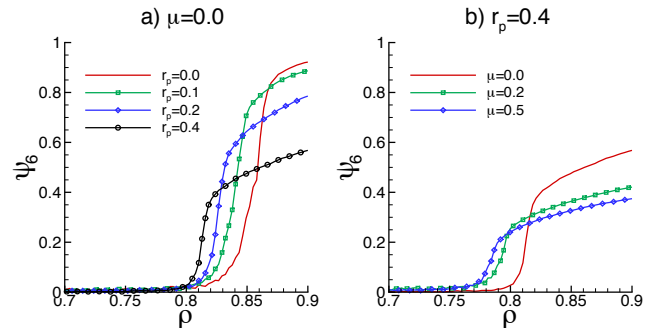


FIG. 8: (Color online) Bond orientational order parameter, ψ_6 , for a) frictionless system with different polydispersity r_p , and b) different friction coefficient, μ , for polydispersity $r_p = 0.4$.

perfect crystal with a hexagonal structure, $\psi_6 = 1$, and $\psi_6 \sim 1/N$ for a disordered system or gas phase. Figure 8 shows that for small ρ 's, ψ_6 is small, and then it increases

for larger ρ 's. The transitional zone occurs at different values of ρ for different systems, and, in particular, the transitional value of ρ decreases as r_p and μ increase. By comparison with the values for jamming transition, ρ_c , given in Table I, we see that the transition in ψ_6 occurs at or very close to ρ_c . As expected, ψ_6 indicates the highest level of ordering for the monodisperse frictionless system.

Note that ψ_6 provides slightly different information from $g(d)$. Figure 8(a) indicates a similar amount of order for the frictionless systems with $r_p = 0.0$ and $r_p = 0.1$, consistently with $g(d)$. However, $r_p = 0.2$ still contains a high level of order which was not clearly apparent from $g(d)$, shown in Fig. 7(a). In any case, neither of the measures captures the non-monotonous dependence of the force network properties on r_p , as found using persistence. Furthermore, Fig. 7(b) shows that $g(d)$ is not influenced by μ for $r_p = 0.4$ and for the considered range of μ 's. On the other hand, Fig. 8(b) shows that ψ_6 reaches somewhat lower value as μ increases. Therefore, in this case the information obtained from ψ_6 appears to be more insightful, since it suggests some difference between frictionless and frictional systems for large polydispersity, consistently with the persistence results.

Based on the above, the bond orientation factor and pair correlation function turn out to provide only limited and to a certain degree inconsistent information, and clearly do not correlate with many of the features of the force networks found using persistence, suggesting that the properties of the force network are not necessarily related to the spatial organization of the particles.

We proceed to discuss a standard measure used to describe global properties of force networks, $P(\bar{F})$, measuring the probability that a particle experiences a (normal) force of a given magnitude. This measure has been explored extensively, see, e.g., [1, 2, 10–12]. In this paper we do not attempt to discuss the influence of order, friction, or other parameters on $P(\bar{F})$ in any depth: we only ask whether the insight reached by the persistence goes further than the one that can be developed based on $P(\bar{F})$, and also whether the corresponding insights are consistent.

Figure 9 shows the evolution of $P(\bar{F})$ for different ρ 's, and for the four frictionless systems shown in Fig. 5. As systems are compressed, we see the transition to a Gaussian-like behavior of $P(\bar{F})$. The results are consistent with the other works that explored the properties of force networks, see e.g. [2]. One observation of interest is that this transition is more pronounced for larger polydispersities; in particular for the monodisperse system the decay of $P(\bar{F})$ appears exponential at large \bar{F} for all considered ρ 's, at least in the considered range (see [12] for much more in-depth discussion of the behavior of $P(\bar{F})$ for very large \bar{F}). To connect now to the earlier discussion, we find that for the systems considered, $P(\bar{F})$ does not capture the features of the force network obtained using persistence. In particular, the evolution of the force network properties that is captured by $P(\bar{F})$

is monotonous as r_p is modified, in contrast to the one found based on persistence. This observation shows that the persistence provides additional information that is not captured by the commonly used measure for quantifying force networks.

Figure 10 shows $P(\bar{F})$ for systems characterized by the same polydispersity, $r_p = 0.4$, but with varied friction (see Fig. 9(d) for $\mu = 0$ case). The results show increased Gaussian-like features of the forces as friction is increased. By careful inspection of $P(\bar{F})$ we see that for large \bar{F} , $P(\bar{F})$ for $\mu = 0$ is large compared to $\mu > 0$ systems. This finding is consistent with the results obtained using persistence diagrams and given in Fig. 6, although the result is not as obvious.

IV. CONCLUSIONS

This work illustrates the utility of computational homology in describing complex features of the force networks in DGM in a clear and concise manner. Use of persistence diagrams to quantify the landscape defined by the contact forces leads to new conclusions regarding the properties of these networks, which may be difficult or impossible to reach by other existing measures. One key feature is the ability to reduce the information encoded by the force network at a particular packing fraction ρ to eight numbers, $N_i^*(\rho)$. The evolution of $N_i^*(\rho)$ as a granular system is compressed provides significant and in the same time tractable information about the evolution of force networks. We find that friction has a crucial role in determining force network landscape: the number of extreme features for $\mu = 0$ is significantly larger compared to $\mu > 0$ case: in other words, the force landscape for $\mu = 0$ is characterized by much larger number of isolated ‘mountain peaks’; these peaks are smoothed by friction. The dependence of the force network properties on polydispersity is not less interesting: we find that small polydispersity leads to significantly larger number of extreme features than the systems that are either monodisperse or strongly polydisperse. This finding cannot be seen when considering other measures, such as force probability density function.

We consider in this work a simple 2D system of compressed disks, but the potential of the described approach is much wider since it is not limited by the physical dimension, by the shape or other properties of the particulate media, or by the type of the flow (compression, shear). We expect that computational homology will provide a significant insight to the force network structure in more complex granular settings, as well as in other soft matter systems, such as colloids, emulsions, or foams.

Acknowledgments: We thank Vidit Nanda for valuable technical assistance with Perseus and R.P. Behringer, J. Dijksman and J. Ren for useful discussions. We acknowledge the support by NSF DMS-0835611, DTRA 1-10-1-0021 (AG, LK); and NSF DMS-0915019, CBI-0835621 and contracts from DARPA and AFOSR (MK, KM).

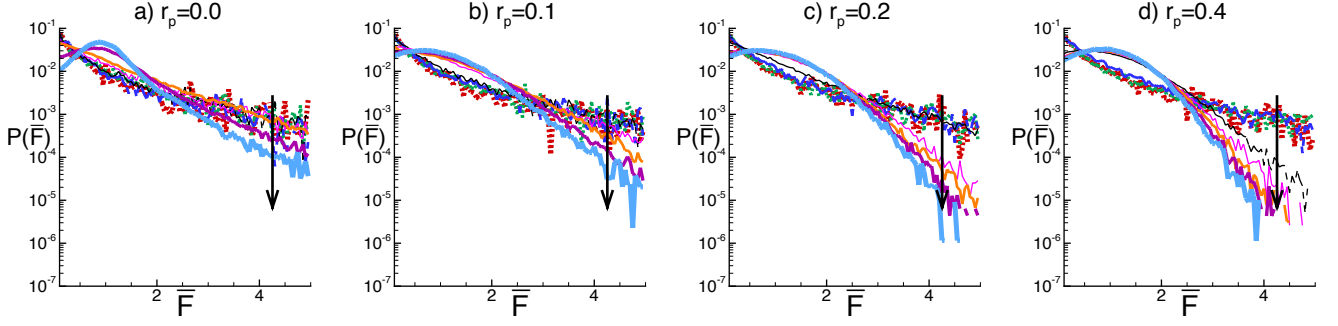


FIG. 9: (Color online) Probability density function, $P(\bar{F})$ for the four systems shown in Fig. 5 ($\mu = 0$). The $P(\bar{F})$ are plotted in $\rho = 0.02$ intervals in the range $[0.76 : 0.90]$, with the results for lowest and highest ρ shown by thick dotted and solid lines, respectively; the arrows show the direction of increased ρ . Note the transition to Gaussian-like form visible in particular for larger r_p as ρ increases.

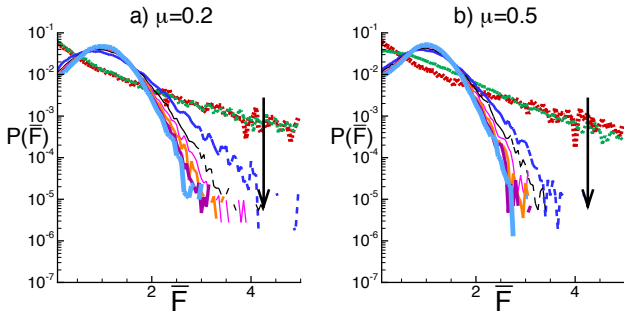


FIG. 10: (Color online) Probability density function, $P(\bar{F})$ for the systems shown in Fig. 6 ($\mu = 0$ is given in Fig. 9(d)). The $P(\bar{F})$ are plotted in $\rho = 0.02$ intervals in the range $[0.76 : 0.90]$. The arrows show the direction of increased ρ . Note that the transition to Gaussian-like form as ρ increases is much stronger compared to $\mu = 0$ cases shown in Fig. 9.

Appendix A: Discrete Element Simulations (DES)

In the simulations, which are two-dimensional, circular grains are confined to a square domain with rough walls composed of monodisperse particles. The walls move inward at constant speed v_c , which yields packing fractions in the range 0.6 to 0.9. No annealing of the system is carried out, and gravity is neglected. The disk sizes are chosen from a flat distribution with width $r_p = (r_{max} - r_{min})/r_{ave}$, where r_{ave} is the mean particle radius. The particle-particle (and particle-wall) interactions include normal and tangential components. The normal force between particles i and j is $\mathbf{F}_{i,j}^n = k_n x \mathbf{n} - \gamma_n \bar{m} \mathbf{v}_{i,j}^n$, where $r_{i,j} = |\mathbf{r}_{i,j}|$, $\mathbf{r}_{i,j} = \mathbf{r}_i - \mathbf{r}_j$, $\mathbf{n} = \mathbf{r}_{i,j}/r_{i,j}$, and $\mathbf{v}_{i,j}^n$ is the relative normal velocity. The amount of compression is $x = d_{i,j} - r_{i,j}$, where $d_{i,j} = (d_i + d_j)/2$, d_i and d_j are the diameters of the particles i and j . All quantities are expressed using the average particle diameter, d_{ave} , as the lengthscale, the binary particle collision time $\tau_c = \pi \sqrt{d_{ave}}/(2gk_n)$ as the time scale, and the average particle mass, m , as the mass

scale. \bar{m} is the reduced mass, k_n (in units of mg/d_{ave}) is the spring constant set to a value that corresponds to that for photoelastic disks [20], and γ_n is the damping coefficient [21]. The parameters entering the linear force model can be connected to physical properties (Young modulus, Poisson ratio) as described *e.g.* in [21].

We implement the commonly used Cundall-Strack model for static friction [22], where a tangential spring is introduced between particles for each new contact that forms at time $t = t_0$. Due to the relative motion of the particles, the spring length, ξ evolves as $\xi = \int_{t_0}^t \mathbf{v}_{i,j}^t(t') dt'$, where $\mathbf{v}_{i,j}^t = \mathbf{v}_{i,j} - \mathbf{v}_{i,j}^n$. For long lasting contacts, ξ may not remain parallel to the current tangential direction defined by $\mathbf{t} = \mathbf{v}_{i,j}^t/|\mathbf{v}_{i,j}^t|$ (see, *e.g.*, [23]); we therefore define the corrected $\xi' = \xi - \mathbf{n}(\mathbf{n} \cdot \xi)$ and introduce the test force $\mathbf{F}^{t*} = -k_t \xi' - \gamma_t \bar{m} \mathbf{v}_{i,j}^t$, where γ_t is the coefficient of viscous damping in the tangential direction (with $\gamma_t = \gamma_n$). To ensure that the magnitude of the tangential force remains below the Coulomb threshold, we constrain the tangential force to be $\mathbf{F}^t = \min(\mu_s |\mathbf{F}^n|, |\mathbf{F}^{t*}|) \mathbf{F}^{t*}/|\mathbf{F}^{t*}|$, and redefine ξ if appropriate.

For the initial configuration, particles are placed on a square lattice and given random initial velocities; we have verified that the results are independent of the distribution and magnitude of these initial velocities. The wall particles move at a uniform (small) inward velocity $v_c = 2.5 \cdot 10^{-5}$. We integrate Newton's equations of motion for both the translation and rotational degrees of freedom using a 4th order predictor-corrector method with time step $\Delta t = 0.02$. We consider system sizes from $N = 2000$ to 40000 particles with $k_n = 4 \cdot 10^3$, $e_n = 0.5$, $\mu_s = 0.5$, and $k_t = 0.8k_n$ [24].

Appendix B: Persistence

A complete description of persistent homology is beyond the scope of this paper. For the mathematical details we refer the reader to [14, 15, 25]. Here we restrict

ourselves to a description of our construction of the scalar field, the force network FN, and chain complexes used for the persistent homology computations.

The spatial information about the particle arrangement is represented by means of a graph called the *contact network* that is constructed as follows. Suppose that the system consists of N particles $\{p_i\}_{i=1}^N$ where the radius of the particle p_i is r_i and the position of the center of the particle is given by (x_i, y_i) . The contact network CN is a graph with vertices $\{u_i\}_{i=1}^N$. The edge $\langle u_i, u_j \rangle$ belongs to CN if and only if the particles p_i, p_j are in contact, that is $(x_i - x_j)^2 + (y_i - y_j)^2 \leq r_i^2 + r_j^2$. Figure 11(a) shows a typical contact network arising from a collection of 15 particles.

The associated scalar field is a function $f : \text{CN} \rightarrow \mathbb{R}$ that takes constant values on the vertices and the interiors of the edges. The value of f on an edge $\langle u_i, u_j \rangle \in \text{CN}$ is defined to be the magnitude of the normal force between the particles p_i and p_j . The value of f on a vertex $u_i \in \text{CN}$ is defined to be the maximum of $f(\langle u_i, u_j \rangle)$ over all edges $\langle u_i, u_j \rangle \in \text{CN}$. A simple example of such a function f is shown at Fig. 12. Observe that f is piecewise constant but not continuous. Figure 11(b) shows a possible scalar field for the contact network CN shown in Figure 11(a).

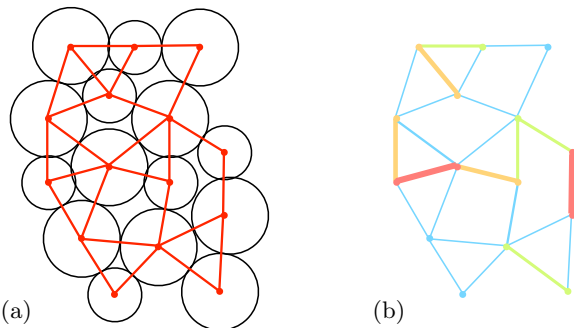


FIG. 11: (Color online) (a) Contact network CN. (b) A scalar field $f : \text{CN} \rightarrow \mathbb{R}$. There are only four different values of f coded by thickness and color. Red (the thickest) line represents the largest value and blue (the thinnest) the smallest one.

Observe that on the level of topology the union of particles in Fig. 11(a) is homotopic to the contact network CN. In particular, this implies that the homology of the set of particles is isomorphic to the homology of CN. In a similar spirit, the dashed lines in Fig. 12 show a continuous function defined on CN which produces the same persistence diagram as that derived from the discontinuous scalar field. This is indicative of the power of homology in the context of data analysis; finite data points provide sufficient information to compute homological invariants for the underlying, but unknown, continuous objects.

In principle we could perform the persistent homology computations beginning with the above mentioned force

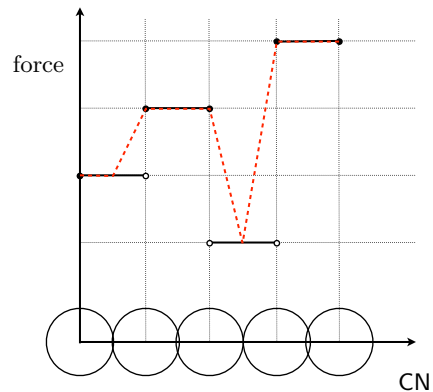


FIG. 12: (Color online) The function f defined on the contact network CN is shown in black. The dashed red line represents the continuous perturbation of f .

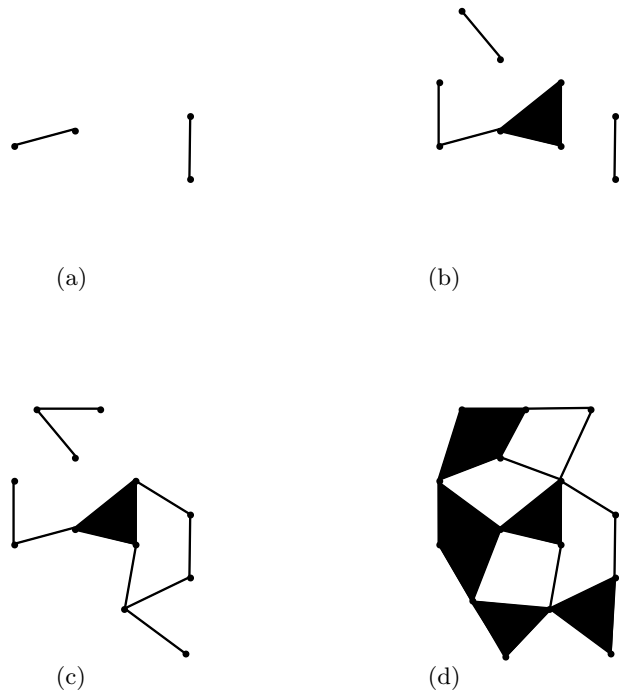


FIG. 13: Four filtrations of the flag complex.

field f . However, we perform two more modifications motivated by the physical application. (1) Force chains are defined in terms of average force. Therefore we normalize the function f by the average force which is computed as a sum of the magnitudes of all forces acting between the particles divided by the number of forces. (2) Because of the finite size of the particles, three adjacent particles always form a loop. We are not interested in counting these loops and are more interested in what we called *defects*, loops that are generated by n -gons where $n \geq 4$. Thus we

form the *flag* complex of CN, that is every triangular hole in CN is filled in with a two simplex σ . The function f is extended to this simplex by assigning it the smallest value that f assumes on the edges of σ . This extension ensures that the force network $\text{FN}(f, \theta)$ is a filtration and we can apply persistence homology. We recall that $\text{FN}(f, \theta)$ is a filtration if $\text{FN}(f, \theta)$ is a complex for every θ (boundary of each simplex in $\text{FN}(f, \theta)$ belongs to $\text{FN}(f, \theta)$) and $\text{FN}(f, \theta_1) \subseteq \text{FN}(f, \theta_2)$ for $\theta_2 \leq \theta_1$. Figure 13(d) indicates the flag complex of the contact network CN of Fig. 11.

Since in our example the force field f takes on only four values, there are only four different values $\theta_1 < \theta_2 < \theta_3 < \theta_4$ for which the force network $\text{FN}(f, \theta)$ changes. The associated force networks $\text{FN}(f, \theta_i)$ are shown in Fig. 13. In our applications to DGM the function f can have as many different values as the number of forces acting between the particles. These forces are used to determine the filtration on which the persistence diagram is computed. This is the filtration which is taken as the input to program Perseus [18].

-
- [1] F. Radjai, D. E. Wolf, M. Jean, and J.-J. Moreau, *Phys. Rev. Lett.* **80**, 61 (1998).
- [2] T. S. Majmudar and R. P. Behringer, *Nature* **435**, 1079 (2005).
- [3] B. P. Tighe and J. Vlugt, *J. Stat. Mech.* **11**, 04002 (2011).
- [4] J. Peters, M. Muthuswamy, J. Wibowo, and A. Tordesillas, *Phys. Rev. E* **72**, 041307 (2005).
- [5] S. Ostojic, E. Somfai, and B. Nienhuis, *Nature* **439**, 828 (2006).
- [6] D. Walker and A. Tordesillas, *Phys. Rev. E* **85**, 011304 (2012).
- [7] A. Tordesillas, D. M. Walker, and Q. Lin, *Phys. Rev. E* **81**, 011302 (2010).
- [8] M. Herrera, S. McCarthy, S. Sotterbeck, E. Cephas, W. Losert, and M. Girvan, *Phys. Rev. E* **83**, 061303 (2011).
- [9] J. W. Landry, G. S. Grest, L. E. Silbert, and S. J. Plimpton, *Phys. Rev. E* **67**, 041303 (2003).
- [10] L. E. Silbert, D. Ertaz, G. S. Grest, T. C. Halsey, and D. Levine, *Phys. Rev. E* **65**, 031304 (2002).
- [11] L. E. Silbert, *Phys. Rev. E* **74**, 051303 (2006).
- [12] A. R. T. van Eerd, W. G. Ellenbroek, M. van Hecke, J. H. Snoeijer, and T. J. H. Vlugt, *Phys. Rev. E* **75**, 060302 (2007).
- [13] L. Kondic, A. Goulet, C. O'Hern, M. Kramar, K. Mischaikow, and R. Behringer, *Europhys. Lett.* **97**, 54001 (2012).
- [14] G. Carlsson, *Bull. Amer. Math. Soc. (N.S.)* **46**, 255 (2009), ISSN 0273-0979.
- [15] H. Edelsbrunner and J. L. Harer, *Computational topology* (AMS, Providence, RI, 2010), ISBN 978-0-8218-4925-5.
- [16] R. Arévalo, I. Zuriguel, and D. Maza, *Phys. Rev. E* **81**, 041302 (2010).
- [17] See Supplemental Material including animations of the force networks and persistence diagrams at [URL will be inserted by publisher].
- [18] V. Nanda, *Perseus* (2012), URL <http://www.math.rutgers.edu/~vidit/perseus.html>.
- [19] K. Mischaikow and V. Nanda, Preprint (2011).
- [20] J. Geng, R. P. Behringer, G. Reydellet, and E. Clément, *Physica D* **182**, 274 (2003).
- [21] L. Kondic, *Phys. Rev. E* **60**, 751 (1999).
- [22] P. A. Cundall and O. D. L. Strack, *Géotechnique* **29**, 47 (1979).
- [23] L. Brendel and S. Dippel, in *Physics of Dry Granular Media*, edited by H. J. Herrmann, J.-P. Hovi, and S. Luding (Kluwer Academic Publishers, Dordrecht, 1998), p. 313.
- [24] C. Goldenberg and I. Goldhirsch, *Nature* **435**, 188 (2005).
- [25] S. Weinberger, *Notices Amer. Math. Soc.* **58**, 36 (2011), ISSN 0002-9920.